Analysis of Thickness Variation in Biological Tissues Using Microwave Sensors for Health Monitoring Applications

SYAIFUL REDZWAN MOHD SHAH[1], (Student Member, IEEE),
NOOR BADARIAH ASAN[1,2], (Student Member, IEEE),
JACOB VELANDER[1], (Student Member, IEEE), **JAVAD EBRAHIMIZADEH**[1],
MAURICIO D. PEREZ[1], (Member, IEEE), **VIKTOR MATTSSON**[1], (Student Member, IEEE),
TACO BLOKHUIS[3], **AND ROBIN AUGUSTINE**[1], (Member, IEEE)

[1]Ångström Laboratory, Solid State Electronics Division, Microwaves in Medical Engineering Group, Department of Engineering Sciences, Uppsala University, SE 75121 Uppsala, Sweden
[2]Faculty of Electronic and Computer Engineering, Universiti Teknikal Malaysia Melaka, Durian Tunggal 76100, Malaysia
[3]Maastricht University Medical Center, Traumatology Department, 6229 HX Maastricht, The Netherlands

Corresponding authors: Syaiful Redzwan Mohd Shah (syaiful.redzwan@angstrom.uu.se) and Robin Augustine (robin.augustine@angstrom.uu.se)

ABSTRACT The microwave sensing technique is a possible and attractive alternative modality to standard X-rays, magnetic resonance imaging, and computed tomography methods for medical diagnostic applications. This technique is beneficial since it uses non-ionizing radiation and that can be potentially used for the microwave healthcare system. The main purpose of this paper is to present a microwave sensing technique to analyze the variations in biological tissue thickness, considering the effects of physiological and biological properties on microwave signals. In order to fulfill this goal, we have developed a two-port non-invasive sensor system composed of two split ring resonators (SRRs) operating at an Industrial, Scientific, and Medical (ISM) frequency band of 2.45 GHz. The system is verified using the amplitude and phase of the transmitted signal in ex-vivo models, representing different tissue thicknesses. Clinical applications such as the diagnosis of muscular atrophy can be benefitted from this study.

INDEX TERMS Microwave sensors, split ring resonators (SRRs), signal loss, biomedical applications, muscular atrophy, sarcopenia.

I. INTRODUCTION

The outcomes of low muscle mass are often dismal and include more surgical complications, prolonged hospital stays, poorer physical function, lower quality of life, and a reduced lifespan. In secondary care such as geriatric and home care, the quality of life of aging people is hampered by a decline in muscle mass, with an increased risk of falling, increased morbidity from diseases, and a decreased life expectancy. A recent systematic review studying populations aged over 50 revealed a prevalence of 1–29 % among community-dwelling populations, 14–33 % among long-term care populations, and 10 % among the acute hospital-care population [1]. The decline of muscle mass (sarcopenia) is recognized as a significant medical risk factor for mortality and morbidity. The total number of people with sarcopenia in Europe was calculated to increase from 19.7 million in 2016 to more than 32 million in 2045 [2]. Sarcopenia can be prevented or treated by physical activity and nutritional intervention.

Although these interventions are cost-effective, the condition has to be diagnosed before any treatment can be initiated and continuously optimized based on the patient's body composition and treatment profile. In several widely adopted

The associate editor coordinating the review of this manuscript and approving it for publication was Qingxue Zhang.

definitions, bioimpedance, ultrasound, computed tomography (CT) scanning, and muscle function determined by mobility tests or strength tests are all used. None of these tests show high accuracy or reproducibility, leading to under-diagnosis of sarcopenia. Bioimpedance technique depends on the electrolyte present in the body fluids, which can vary highly depending on the hydration level of the patient. CT scanning, on the other hand, uses ionizing X-ray radiation and is not suitable for frequent use. Ultrasound results are largely operator-dependent; therefore, it is difficult to obtain objective and quantitative results for muscle variations. In addition, all current aforementioned approaches can be bulky and costly to enforce, and there is often still a necessity for an experienced operator to take time to consider the significance of the outcomes achieved. This is inappropriate during an operation as time is often critical from the perspective of a patient's well-being and hospital efficiency.

Microwave sensing is a technology that has demonstrated enormous potential in a variety of industrial and medical fields [3]–[5]. This is because the technique is robust, requires low power, has high sensitivity, is non-invasive, and has a good penetration depth in terms of material analysis compared to other state-of-the-art modalities. The non-ionizing nature of microwave radiation, which practitioners see as a important advantage over current techniques such as CT scanning and X-ray imaging, is also a benefit of using microwaves for medical applications.

Our present work uses the microwave sensing technique to understand the geometrical distribution of a multi-layered tissue by calculating the signal loss while the signal is propagating through tissues. A primary concern here is the received signal's signal-to-noise ratio (SNR), which requires the underlying multilayer human body that governs the microwave propagation, and its impact on attenuation to be resolved so that microwave sensing systems are designed and implemented accurately. One of the main considerations of these requirements is the study of EM signal propagation characteristics on body tissues. Microwave propagation is then investigated based on tissue dielectric properties in terms of reflection, signal loss, attenuation, and penetration depth.

The feasibility of the microwave sensing technique is examined using microstrip split ring resonators (SRRs) to estimate the EM signal loss through biological tissues. Two prototypes consisting of three layers of tissue thicknesses (skin, fat, and muscle) are presented primarily for the measuring conditions and personal characteristics of human tissues. This paper requires an analytical approach to examine the influence of the tissue proportions on the EM signal coupling.

To verify the outcomes, a laboratory setup comprising of two SRR sensors and an ex-vivo porcine experimental model for biological tissues are introduced. We also carried out an intensive parametric analysis of a variety of fat and muscle thickness values at different sensor distances, which enabled us to conclude the underlying EM signal coupling. Finally, a validation was achieved between the electric field (E-field) and penetration depth and their associated effects on signal loss due to the variation in thickness and distance. The paper is organized according to the following sections: section I is the introduction to the study; section II describes the outline of materials and methods used in the proposed work, including the use of numerical and ex-vivo models of the experimental setup; section III compares and discusses the simulated and measured results of the two SRR sensors. Finally, section IV summarizes the conclusions of this paper.

II. MATERIALS AND METHODS
This paper studies the signal coupling for on-body microwave propagation through various biological living tissues and validates the influence of the tissue thickness. Ultrasound (US) images are used to obtain the layer thicknesses and compositions of skin, fat, and muscle tissues. The collection of data was carried out using ethical approval from Sweden (2016/698 - 31/1). The numerical simulation models are made using human US information and are validated using the equivalent ex-vivo model.

A. DESIGN OF THE SPLIT RING RESONATOR SENSOR
In this work, a microwave split ring resonator (SRR) sensor loaded with biological tissues, which operates in the 2.40–2.48 GHz Industrial, Scientific, and Medical (ISM) frequency bands, is presented. The frequency band was selected as it is commonly used in ultra-wideband standards IEEE 802.15.4a. Previous publications have shown that an SRR-based approach is the most promising in this field for several reasons [6]–[8]. The sensors comprises a resonator and a matching substrate layer. The fundamental principle behind its operation is that variations in the human tissues will produce variations in the effective permittivity of the microstrip resonator and, hence, a variation in its resonance. Therefore, it will provide a potential correlation between a resonance state and a state of a particular change in the dielectric properties of tissues. Perez *et al.* in [9], [10] demonstrated, through an ethically approved trial in human volunteers, that sensors made with this type of resonator could have a signal low enough to ensure a secure tissue absorption but high enough to ensure penetration into human tissues of about 15 mm, capable of reaching muscle and bone tissues in some cases.

This concept is also supported by other studies including, besides an assessment of burn injuries [11], ethically approved clinical trials studying bone healing after cranial [12], [13] and hip fracture surgeries [6], [8], [14]. In addition, as part of future optimization and system integration processes, an analytical model is also proposed and being studied [15].

The split ring resonator sensor design uses the concept of a single split microstrip ring resonator (known as microstrip gap) as illustrated in Fig. 1(a). Model parameters used to develop the split ring resonator are shown in Table 1. We used three different layers of the substrate to design the split ring resonator sensors. Layer 1 is a ground plane with thickness $h_1 = 0.035$ mm. Layer 2 with thickness h_2 is made of
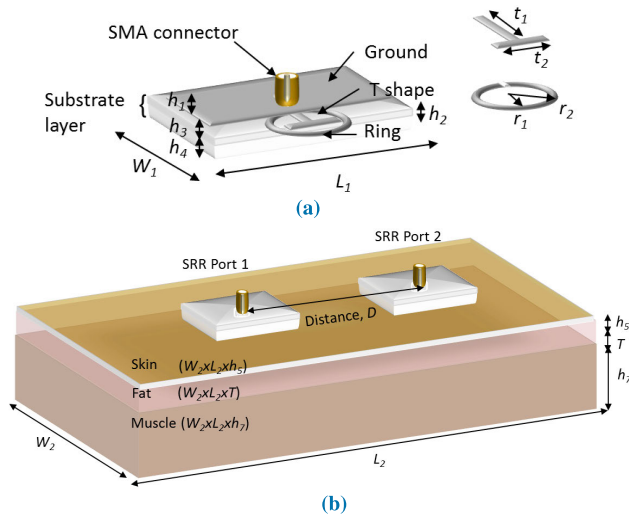
FIGURE 1. (a) Geometry of the SRR sensor and (b) Multilayer structure tissues with distance variation between Tx and Rx SRR sensors used for biological tissue characterization.

TABLE 1. Model parameters used for investigating signal transmission in biological tissues.

Categories	Type	Label	Dimension (mm)
Split Ring Resonator	Ground	h_1	0.035
	Substrate	W_1	25
		L_1	25
		h_2	0.635 (TMM4)
		h_3	0.635 (TMM6)
		h_4	0.635 (Roger 6010)
	Ring Resonator	r_1	8.6
		r_2	5.8
	T-shape	t_1	9.2
		t_2	4.2
Tissues	Skin	T_5	2.3
	Fat	T	5–35
	Muscle	h_7	10–50
	Width	W_2	120
	Length	L_2	250

TMM4 substrate ($\epsilon_r = 4.5$, loss tangent, $\tan \delta = 0.002$) in which thickness $h_2 = 0.635$ mm, and layer 3, h_3 with TMM6 substrate ($\epsilon_r = 6$, loss tangent, $\tan \delta = 0.0023$) with thickness $h_3 = 0.635$ mm. Both layers 2 and 3 are fabricated using TMM high-frequency laminates. In addition, layer 4 with thickness h_4 is fabricated using Rogers 6010 substrate ($\epsilon_r = 10.2$, loss tangent, $\tan \delta = 0.0023$) in which thickness $h_4 = 0.635$ mm, forming a total thickness of about 1.905 mm. In the lab prototype, all the layers were stacked and glued together using adhesive glue. Specifically for layer 4, we used this as a matching layer principally made up of a substrate sheet, which performs as a coupling material to the target (which is the skin tissue) and makes it possible to radiate more EM waves into the biological tissues and achieve stable resonance frequency while illuminating the targets.

The structure of the SRR has been proved to have a penetration depth between 10 and 15 mm when applied on the

surface of the skin in distal and thigh positions (upper part of the leg-femur) as shown by Mohd Shah *et al.* [6] and [8] on human volunteers. Each tissue is characterized by the differences in dielectric properties, focusing primarily on relative permittivity, ϵ_r, and conductivity, σ.

In particular, the conductivity of skin and muscle tissues at high frequencies is much higher than the conductivity of the fat tissue. This is because of the high water content in the skin and muscle compared to the low content of water in fat and bone. Our work is complementary to this approach. The signal connection was chosen to be perpendicular to the ring's plane and at the center of the ring's projection on the ground plane. Therefore, a SubMiniature version A (SMA) connector is employed and the signal's transition to a microstrip line starts from the bottom (ground) in the center of the ring's projection and to the edges of the parallel section of T-shape microstrip line. The sensor input impedance is optimized to be close to 50 Ω. All these aspects have been verified with the help of Computer Simulation Technology (CST Studio, 2018, DASSAULT SYSTÈMES, France).

B. NUMERICAL SIMULATION ANALYSIS

For this purpose, we demonstrated the development of two 3-D models using the CST software based on US tissue thickness measurements. Fig. 1(b) illustrates the suggested arrangement that is used to characterize the EM signal loss on the biological tissues. To study the interaction of the proposed sensors and ex-vivo model, a transmitter sensor (Tx) is placed to create an EM signal that perpendicularly propagates into multilayer tissues; meanwhile, a receiver sensor (Rx) performs to identify the received EM signal. The geometrical thickness of each tissue layer, which includes the numerical and experimental ex-vivo, is listed in Table 1. Biological tissue properties included in the simulation are applied at a frequency of 2.45 GHz to excite the behavior of three tissue layers depending on the thickness tissue.

In this study, our approach is to develop a multilayer homogeneous model that has been considered for numerical and experimental studies. This model consists of a three-layer tissue with different thicknesses containing skin, h_5, fat, T, and muscle, h_7. Here, the skin thickness is kept constant (2.3 mm), while the fat and muscle thicknesses are varied from 5 mm to 35 mm in 10 mm steps and from 10 mm to 50 mm in 20 mm steps, respectively. The length of the simulation model is 250 mm and the width is 120 mm, which optimizes the condition for signal loss. As mentioned earlier, human tissues can be classified into those with high water content (like muscle and skin) and those with low water content (like fat). Therefore, the influences of fat and muscle thicknesses on the EM signal loss between the transmitter and receiver sensors are examined and analyzed. A transmitter sensor generates an EM signal perpendicularly propagating through the other upper tissue layer, while a receiver sensor is used to detect the received signal by varying the distance between them from 0 mm to 250 mm in 50 mm steps.
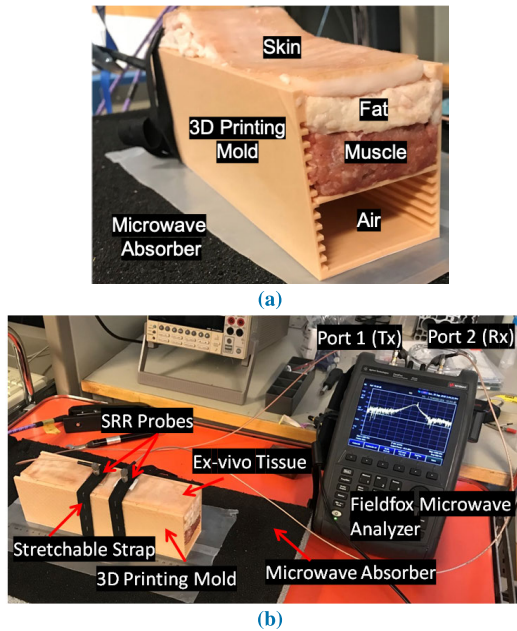
(a)

(b)

FIGURE 2. Photographs of the ex-vivo experimental setup. (a) Multilayer homogeneous model containing skin, fat, and muscle of ex-vivo porcine tissues and (b) Two-port system with different distance positions of Tx and Rx SRR sensors. The ex-vivo multilayer model is the arrange inside a custom-made container to suit these series of experiments.

C. EX-VIVO AND EXPERIMENTAL SETUP

We emulated human tissues using fresh porcine belly which is commonly used in in-body imaging and power transfer systems [16]–[18]. These tissues have layer structures that are complex and include skin, fat, and muscle. Furthermore, these tissue EM properties are similar to human tissues [19], [20]. This tissue material, therefore, provides an ideal environment for human tissue emulation. The skin, fat, and muscle of porcine belly tissues are separated and finely minced with a meat mincer. The three-layered tissue structure, which contains skin, fat, and muscle (top to bottom), is placed and arranged in a custom-made 3D-printed plastic container and supported by a 5 mm-thick plate below the muscle layer. The size of the mold is 250 mm in length, 60 mm in width, and 80 mm in height. By varying the leveling plate underneath the muscle layer, the thicknesses of the fat and muscle layers in the ex-vivo tissue can be changed. On the other hand, a flexible, broadband, lightweight, and multilayer flat carbon loaded laminate polyurethane (PU) foam-based microwave absorber is used for the experimental setup (FU-ML-120, Sahajanand Laser Technology Ltd, Gujarat, India). The dimension of the microwave absorber are 600 mm in length, 600 mm in width and 120 mm in height, and its reflectivity performance is −17 dB at 2.0 GHz. Fig. 2(a) shows a picture of this experimental setup.

The SRR sensors are attached to the surface of the skin layers by using a stretchable strap to ensure that the sensor remains in sufficient contact with the skin and retains constant pressure throughout the measurement. The sensors are then aligned as shown in Fig. 2(b) and connected to the Fieldfox

Microwave Analyzer (N9918A). The measurement is conducted in the frequency range of 1–4 GHz and the resonance frequency of the sensor is optimized at 2.35 GHz in a normal condition (skin = 2.3 mm, fat = 5 mm and muscle = 10 mm). In order to investigate the signal loss, S_{21} through the tissues, the distance between the two SRR sensors is varied from 0 mm to 250 mm during the measurement. These distances are chosen based on the clinical US measurement adopted in previous studies [6]–[8].

Additionally, this ex-vivo model is examined to gauge the depth of penetration by analyzing the E-field distribution of the layered tissues. Inferences from the E-field distribution simulation are made to characterize the signal loss in the experimental setup and the results are compared. The penetration depth provides good information for analyzing sensor performance especially the E-field distribution in different tissues, and can be used for future work in clinical measurements.

D. ON-BODY AND IN-BODY SIGNAL PROPAGATION

The electromagnetic (EM) waves mainly propagate around the human body surface via diffusion. As an outcome, the human body, a high-loss dielectric medium, usually has huge impacts on the signal propagation. Additionally, as human tissues contain a range of dielectric properties, a functional model of the body would need to be studied on the signal propagation. Specifically, when RF signals propagate from a high dielectric property medium (like skin or muscle) to a low dielectric property medium (like fat), it bends away from the direction perpendicular to the interface between the materials. This means that any signal that is propagated into the body has to travel across multiple centimeters (cm) of multilayer tissues and faces multiple reflections before it can exit to the air, as shown in Fig. 3. Thus, signal propagation in each layer is assumed to be linear, but across layers, it can change to multiple directions. To validate the effects of fat and muscle layer variation, the thickness of the skin (2.5 mm) layer remains fixed; meanwhile, the variation of the fat thickness is adjusted from 5 mm to 35 mm in 10 mm steps. Furthermore, the variation of the muscle thickness from 10 mm to 50 mm in 20 mm steps is also considered. It is necessary to calculate and sum up the maximum and minimum differences of the magnitude of S_{21}, $|S_{21}|$, required to propagate across each model layer. To calculate the signal loss, the skin and muscle are considered to remain constant and the maximum and minimum signal loss are reckoned by varying the fat layer thickness. Therefore, the different signal loss, S_{21} (in dB), can be calculated by:

$$\Delta_{\text{signalloss}} = \text{Max} - \text{Min} \qquad (1)$$

where $\Delta_{\text{signalloss}}$ is the signal loss, S_{21} (dB), and Max-Min is the difference between the maximum and minimum signal at any variation of the fat and muscle thicknesses.

This will provide a basis for the comparison of approximations that can be used from the human tissue model for
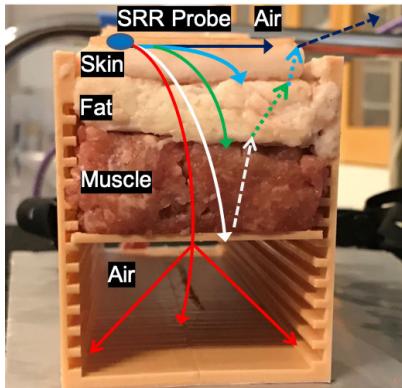
FIGURE 3. Illustration of signal reflection from the multilayer ex-vivo model.

reflectivity and refractivity, and their suitability for integration into larger EM models.

III. RESULTS AND DISCUSSION

In this section, the signal coupling is discussed and divided into three parts within the introduced variation model of thickness and distance. First, a detailed EM signal analysis that focuses on two targeted low and high loss materials, fat and muscle in section III-A is conducted. S_{21} results are obtained and presented in this section for simulation and ex-vivo measurements. The multilayer model for E-field distribution is analyzed in section III-B. Additionally, an estimation of penetration depth is studied and presented in section III-C to investigate the sensor's performance concerning the E-field distribution.

A. SIGNAL LOSS ANALYSIS

In this subsection, a numerical study is performed to demonstrate that an SRR has the sensing capability with which multilayer tissues can be analyzed. The SRRs are placed above the body tissue, which is a multilayer medium consisting of air, skin, fat, and muscle, to couple the EM signal inside the body tissue. The distance between the two SRRs are varied

from 20 mm to 160 mm, and the amplitude and phase of the coupled signal for the fat layer are reported.

As shown in Fig. 4(a), the SRRs do not resonate in free space; however, when the SRR is located over the body tissue, it resonates at a central frequency of 2.35 GHz. So, the SRR is sensitive to the characteristic parameters of the body tissue; as soon as the tissue parameters vary, a significant variation in the resonance frequency of the resonator occurs.

To calculate the free space coupling of the SRRs, two simulations are conducted. In the first simulation, the two SRRs are placed apart from each other and are connected with the free space channel and in the second simulation, they are placed on the body tissue. Fig. 4(b) shows the coupling between the two SRRs. For the case of free space, it is observed that at the resonance frequency of 2.35 GHz, the coupling through free space is below −90 dB and the coupling through body tissue is −14 dB. Therefore, it is clear that the SRR has the potential to couple the EM signal inside the fat layer compared to the coupling through free space. The entire signal coupling is done through the body channel. With an increase in distance between the two SRRs, there will be an increase in path loss. However, the path loss is nonlinear because the system is a near-field system.

To analyze further, the variation of distance between the SRR sensors, which is increased from 20 mm to 250 mm, is investigated. Fig. 5(a) and (b) show the results of the amplitude and phase when the thickness of the skin = 2.5 mm, fat = 20 and 35 mm, and muscle = 50 mm. The variation in signal coupling due to the change in the distance gradually decreases to about 8 dB when the SRR distance is increased. However, there is no significant discrepancy in phase variation over different thicknesses. It can be seen that the thickness does not strongly affect the phase of the transmission with respect to the fat layer. The SRRs demonstrate EM coupling but not EM propagating; therefore, no significant phase difference is observed. The amplitude of the signals is affected by the channel thickness.
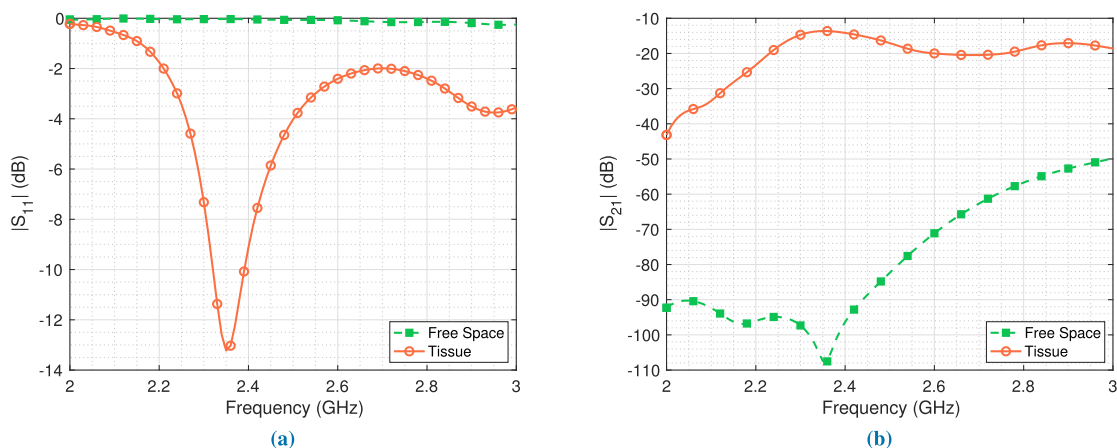

FIGURE 4. (a) The simulated reflection coefficient, S_{11} and (b) The simulated signal coupling, S_{21} between the two SRRs at the distance of 20 mm for two scenarios of free space and body tissue channel.
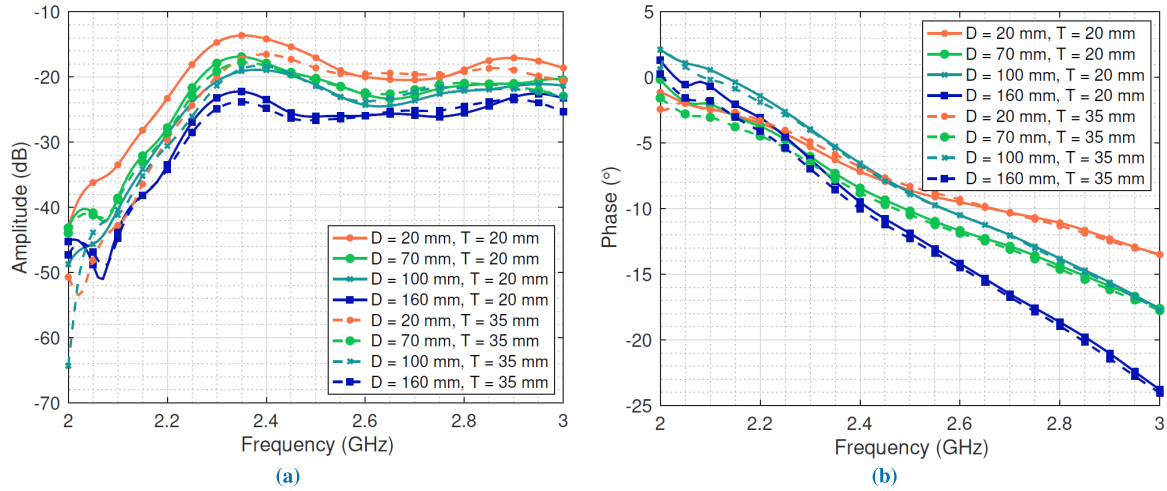
FIGURE 5. The comparison of (a) Amplitude of S_{21} and (b) Phase of S_{21} when the thickness of skin = 2.5 mm, fat = 20 and 35 mm (*T*), and muscle = 50 mm. The SRR sensors placed on top of the skin layer with a gap distance from 20 mm to 160 mm (*D*).
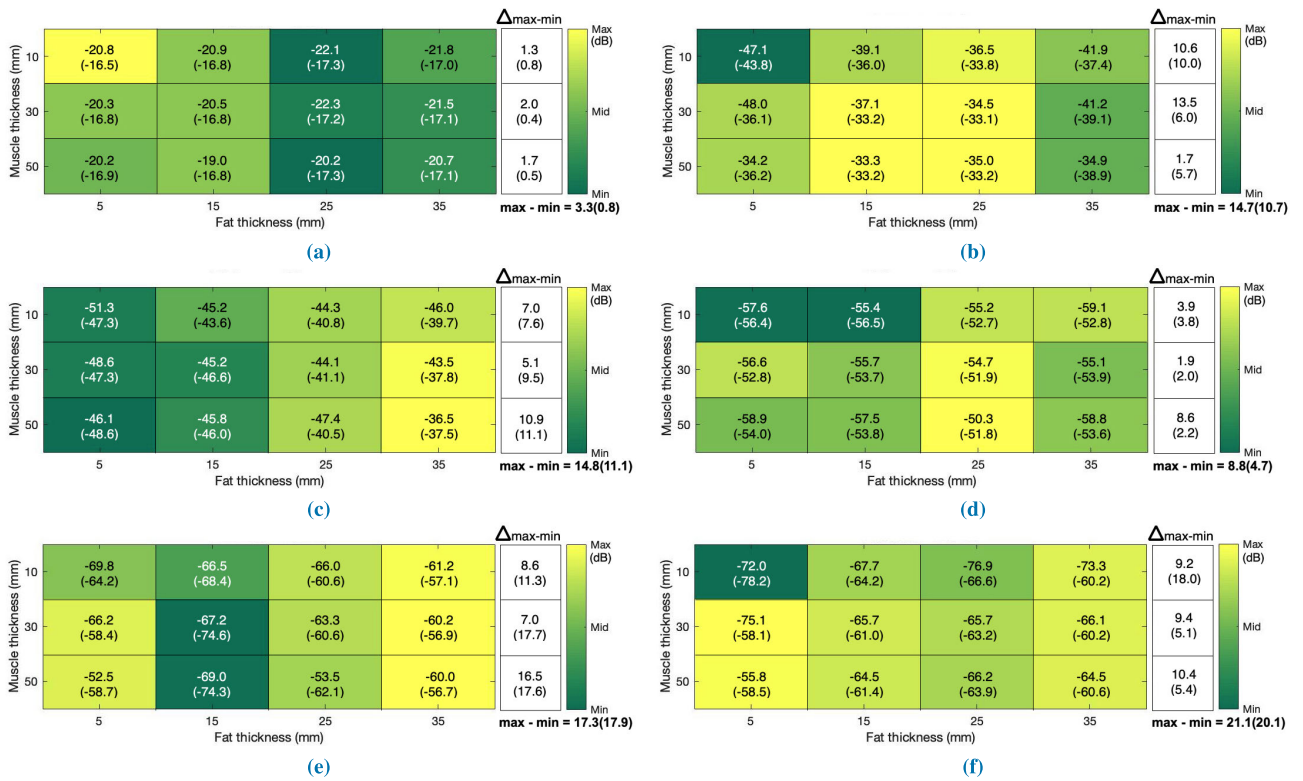

FIGURE 6. The simulated and measured S_{21} results when the thickness of skin = 2.5 mm, muscle thickness varied from 10 mm to 50 mm in 20 mm steps, fat layer varied from 5 mm to 35 mm in 10 mm steps. The SRR sensors placed on top of the skin layer varies with (a) Distance = 0 mm (b) Distance = 50 mm (c) Distance = 100 mm (d) Distance = 150 mm (e) Distance = 200 mm and (f) Distance = 250 mm.

Next, Fig. 6 shows the results of the simulation and measurement of homogeneous layer tissues consisting of skin, fat, and muscle (organized from top to bottom). To characterize the signal loss of the multilayer tissue, the layered fat and muscle tissues are defined as a function of the distance between the two SRR sensors. As illustrated in Figs. 6(a)–(f), the solid values correspond to the results

of the measurements and the values inside the parentheses correspond to the results of the simulation. The colorbar index indicates that color variation corresponds to the measured and simulated S_{21} results (in dB) (within parentheses) from minimum to maximum values.

From the results shown in Fig. 6(a), the observation of signal loss is between 19.0 dB and 22.3 dB for the 0 mm
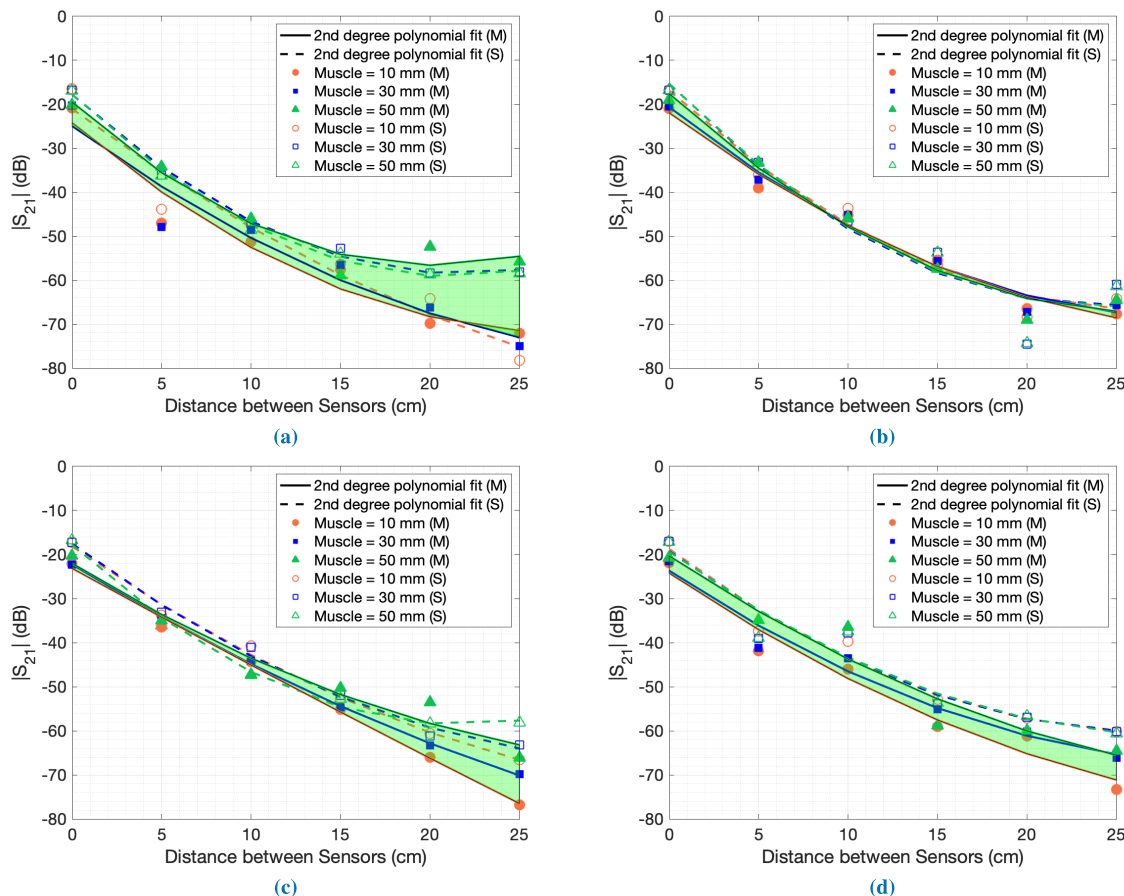
FIGURE 7. The measured and simulated (within parentheses) S_{21} results when the thickness of skin = 2.5 mm, (a) Fat = 5 mm, (b) Fat = 15 mm, (c) Fat = 25 mm, and (d) Fat = 35 mm, respectively for muscle thickness varying from 10 mm to 50 mm in 20 mm steps. The SRR sensors are placed on top of the skin layer and varied with distances from 0 to 250 mm.

distance position. It shows the variability that the fat thickness produces signal loss at the fixed thickness of the muscle. In the 0 mm position, the received signal is significantly reduced by 2.1 dB at 25 mm for the fat-layered tissue case that includes skin and muscle variation. This can be explained by the signal diffusion due to high attenuation and frequency dispersion in the muscle tissue of the microwave signals. In addition, most of the reflection signals in the fat layer dissipate and penetrate to deeper tissue layers.

Furthermore, we observed that the influence of the increasing distance between Tx and Rx sensors as a function of the layered fat and muscle tissue does provide a significant difference in signal loss as shown in Fig. 6(b). The first strong effect is observed at the boundary between thinner fat and muscle, where the magnitude of the signal loss dropped up to −43.8 dB for simulation and −48.0 dB for measurement. As the contrasts between skin and fat as well as between fat and muscle are very high, strong reflections also occur at these two boundaries.

Another notable aspect that can be seen in Fig. 6(c) is that the measured values slightly increased when 35 mm thick of fat and 50 mm of muscle tissue are used. The results show,

for example, that when the muscle remains constant in the thicker layer, it has an attenuation of 9.6 dB/cm in difference. This is in line with expectations mainly caused by EM signals due to their high permittivity and loss; they are significantly reduced before they reach the receiver [21], [22].

On the other hand, the effect of material absorption in these layers can be observed to be slightly lower in relation to the behavior of a strong reflection signal when looking at the thinner layers of fat tissue for all the figures. This is because the fat tissue layers used are much thinner than the corresponding penetration depths (117.1 mm at 2.45 GHz) [19], and once the E-field is confined to the fat limit, it constantly attenuates.

In Fig. 7(a)–(d), a comparison of signal loss is shown for different muscle thicknesses while the fat layer is fixed. The signal loss of 5 mm of fat thickness at a distance of 0 mm with a minimum muscle of 10 mm is 24.2 dB and approximately 20 dB with a maximum muscle of 50 mm. The signal loss increases from 72 dB to 54 dB for maximum and minimum muscle thickness at a distance of 25 cm. Meanwhile, in Fig. 7(d), we observed the signal loss of 35 mm of fat thickness having a smaller variation from 19 dB to 21.5 dB for

maximum and minimum muscle thickness at 0 mm distance and between 68 dB and 64 dB for 25 cm distance. The high contrast in the dielectric properties between the muscle and the fat layer allows even thin muscle layers to act as good boundaries that confine signals within the fat layer. The results of this investigation provide a better understanding of the signal loss and can be utilized to extend or evaluate tissue thickness when a fixed sensor position is applied. The standard deviation of the sensor is ±0.08, which shows that the data points are significantly different from each other.

In addition to Fig. 7(a)–(d), the different fat thickness shows a very distinctive curve/pattern, which could be used to distinguish the thickness of underlying tissues. The distinctive curve has been noted to be significantly influenced by a $1/2\lambda$ of the fat thickness (Fig. 7(a) and (c)), which could be distinguished as muscle variation. From this perspective, the transparent boundary conditions contributes effectively to the wave for it to travel from the fat to the muscle layer. However, when the thickness of fat is increased to $1/4\lambda$ (Fig. 7(b) and (d)), no significant impact on the distinctive curve is observed. Thus, the Salisbury screen phenomenon occurred due to the cancellation of the incident wave at the front of the muscle layer. Taking into account the distance variations, the shorter the distance, the stronger the upper layer interaction. The surface wave is thus observed to have a substantial effect on the mutual coupling between the two SRR sensors.

B. E-FIELD DISTRIBUTION ANALYSIS

In addition to the described attenuation of the signal due to the differences in dielectric properties, the distribution of E-field is presented when propagating from one layer to another. Fig. 8(a)–(c) show a two-dimensional (2-D) E-field distribution by varying the fat thickness. We considered three experimental scenarios to inspect the E-field distribution between the Tx and Rx sensors at a fixed distance of 100 mm:

1) **Scenario 1**: Minimum thickness of the fat layer of 5 mm to represent a thinner condition.
2) **Scenario 2**: An average thickness of the fat layer of 25 mm to represent a normal condition.
3) **Scenario 3**: Maximum thickness of the fat layer of 35 mm to represent a high-fat condition.

Fig. 8(a) shows the E-field distributions of the thinner condition in the fat tissues, which results in higher surface coupling and leakage of the signal. The E-field leaks more outside of the skin layer, from the fat layer to the surrounding free space. In this case, the consideration of multiple reflections can occur between the surface layer and fat tissue boundaries. Therefore, the layer of fat showed an enlargement of the E-field close to the Rx sensor with the prominence of mismatching on the Tx sensor.

In Fig. 8(b), we observed that increasing the thickness of the fat layer enables the E-field to propagate further through the muscle tissues. It is thus observed that the attenuated signal in this layer is small compared to scenario 1 in the
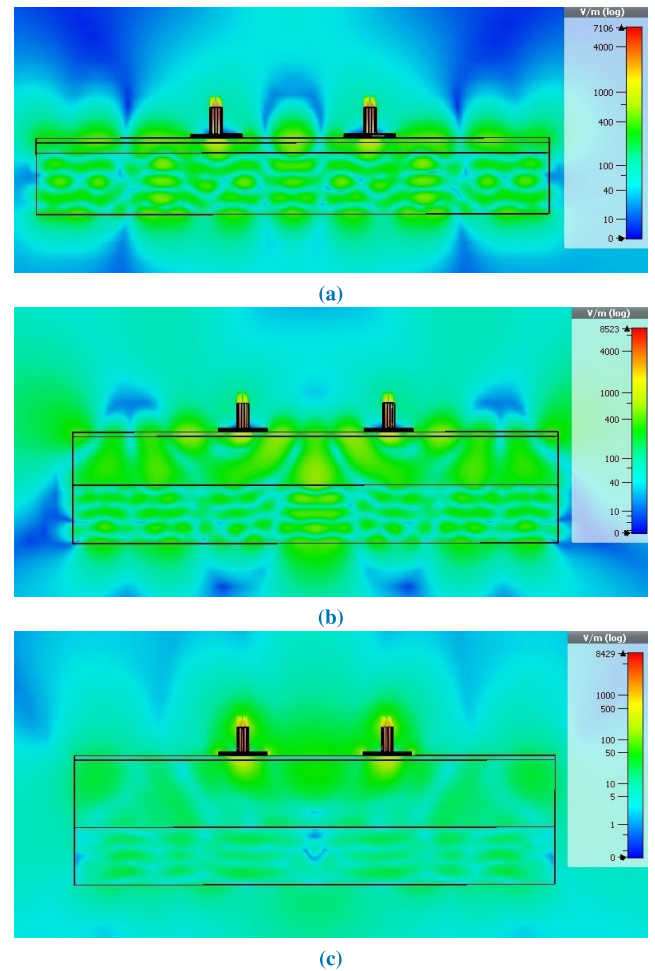
(a)

(b)

(c)

FIGURE 8. The E-field distribution depending on the thickness of the tissue (a) Fat = 5 mm, (b) Fat = 25 mm, and (c) Fat = 35 mm at 100 mm distance from the SRR sensors.

muscle tissue layers of this condition. It is important to note that there are two significant contributions: (i) the loss of absorption due to the material properties, and (ii) the loss of the reflection signal as it propagates through multiple tissue layers.

For the arrangement of scenario 3 (Fig. 8(c)) where the maximum fat tissue thickness is 35 mm, the signal is continuously attenuated for thicker fat as the result sets are very similar to scenario 2. Therefore, we observed that while increasing the fat layer thickness between 25 mm and 35 mm, there is no significant change in E-field distribution through the fat-muscle boundaries. The transmitted RF signal is constantly attenuated while passing through the fat tissue where the attenuation depends on the thickness of the fat. Hence, the reflected signal from the next tissue declines even further and causes the exponential fading of the signal, especially from the beginning of the muscle tissue.

In summary, we observed two types of eigenmodes, namely, the bound states and the free states [23]–[25]. The former are the modes bounded in the fat layer and they trap the signal mainly within the layer between the skin and muscle. The latter are modes that trap the signal of the exterior mode,
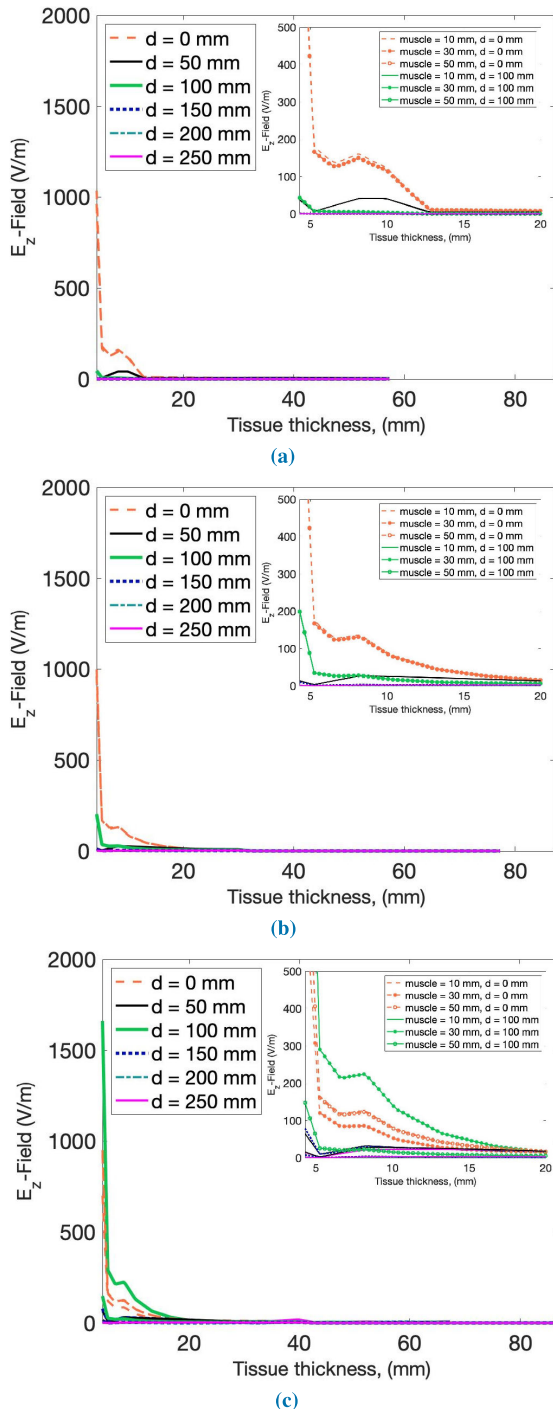
FIGURE 9. The E-field penetration depending on the thickness and variation of distance. (a) Fat = 5 mm, Muscle = 10 mm, 30 mm, and 50 mm (skinny condition), (b) Fat = 25 mm, Muscle 10 mm, 30 mm, and 50 mm (normal condition), and (c) Fat = 35 mm, Muscle = 10 mm, 30 mm, and 50 mm (high-fat condition).

which are not bound to the layered fat but are flowing in the open regions.

C. PENETRATION DEPTH ASSESSMENT

Our objective in this section is to observe the penetration depth by examining the same experimental scenario from the previous section. The examination is done from the simulated E-field and the results are correlated. The actual position of the E-field is obtained from the E_z axis at the Rx sensor. The E-field along the E_z axis perpendicular to the sensor plane is considered. The starting point of the E_z axis is taken at the maximum E-field strength which happens to be at the interface of the sensor and skin surface. The distribution of the E-field is observed along the E_z axis through the different tissue layers of the simulation phantom until the E-field dies off (in the layer of fat).

Fig. 9(a)–(c) show that the similarity in the performance of the penetration depth expands throughout the fat layer (2.5 mm to 10 mm on average on the tissue thickness axis) and the intensity of the E-field rises at the skin-fat boundary. Considering the tissue thickness information, when a thicker fat layer is present, the penetration depth is discovered to be greater. Thus, the thickness of the fat layer is observed to have a great impact on the distribution of the E-field. Because fat tissue has inherently low water content, its dielectric characteristics show very low frequency dispersion. In addition, the extent of the E-field represents the percentage increase in the magnitude of the E-field in the fat layer. Using the following equation, it is calculated as follows:

$$\mathrm{E_{extend}} = \left(\frac{\mathrm{Max}}{\mathrm{Min}} - 1 \right) \times 100 \% \tag{2}$$

On average, 200 V/m (44.5 %) of the E-field intensity increases in the skin-fat boundary and decreases into the next layer. The depth is gradually decreased once the E-field arrives at an average fat thickness of 10 mm.

Another notable aspect to be observed in Fig. 9 is that the E-field initiates to be interrupted approximately 60 mm at the minimum tissue thickness (scenario 1) and extends more than 80 mm for maximum tissue thicknesses (scenario 3). Looking at the multilayer tissue thickness composition of all the graphs in Fig. 9, it can be seen that in the fat-muscle boundary, the material absorption occurs. Therefore, the impact of dielectric properties is very different between the muscle and the fat layers which strongly affects the penetration depth. According to these results, the signal will fluctuate at this depth because of the appearance of reflected signals.

IV. CONCLUSION

In this study, the coupling of RF signals within human body tissue is investigated by considering the physical appearances of a multilayer model development. A method of using microwave microstrip SRR sensors with two prototypes of a three-layer ex-vivo models has been proposed with a varied distance of sensors to measure the signal loss with the resonance method. The S-parameters in the 2.40–2.48 GHz ISM frequency band between the transmitter and receiver sensors are investigated. The EM signal loss is analyzed showing correspondence to the variation of the tissue thickness and distance. Some mechanisms influencing the signal pathways

through tissues have been addressed. 1) The observation shows that the EM signal coupling through thick fat tissue has a coupling loss of 2.1 dB per 20 mm, an average of 25 mm in distance for the ex-vivo model. 2) There are significant variations between distance and E-field distribution. The results becomes especially relevant when compared with penetration depth. The penetration depth at any given distance of two sensors also depends on the thickness of the tissue that has lower conductivity, such as the fat layer. Therefore, the sensor's performance (e.g. impedance matching) is strongly determined by the dielectric properties of the tissues and the structure of the human body. The variation of muscle thickness does not improve much on the reflection and signal loss, which is considered as a result of the losses in dielectric properties of this layer. The included numerical and experimental validations proved the thicknesses of the fat and muscle tissues give a correlation of resonance frequency and signal loss responses. For example, the fat tissue has the lowest relative permittivity of around 5 (at 2.45 GHz), since it has almost insignificant water content. In contrast, the muscle has a higher relative permittivity of 58 due to the presence of high water content in the tissue. Hence, the frequency dependence of the relative permittivity of high water content tissues varies significantly. These proposed sensor and measurement methods can be extensively applied to many practical medical applications.

REFERENCES

[1] A. J. Cruz-Jentoft and J. Alfonso, "Prevalence of and interventions for sarcopenia in ageing adults: A systematic review. Report of the International Sarcopenia Initiative (EWGSOP and IWGS)," *Age Ageing*, vol. 43, no. 6, pp. 748–759, Nov. 2014. doi: 10.1093/ageing/afu115.

[2] O. Ethgen, C. Beaudart, F. Buckinx, O. Bruyère, and J. Y. Reginster, "The future prevalence of sarcopenia in Europe: A claim for public health action," *Calcif Tissue Int.*, vol. 100, no. 3, pp. 229–234, Mar. 2017. doi: 10.1007/s00223-016-0220-9.

[3] D. Wagner, S. Vogt, F. I. Jamal, S. Guha, C. Wenger, J. Wessel, D. Kissinger, K. Pitschmann, U. Schumann, B. Schmidt, and M. Detert, "Application of microwave sensor technology in cardiovascular disease for plaque detection," *Current Directions Biomed. Eng.*, vol. 2, no. 1, pp. 273–277, Sep. 2016. doi: 10.1515/cdbme-2016-0061.

[4] A. Mason, A. Shaw, and A. Al-Shamma'a, "A co-planar microwave sensor for biomedical applications," *Procedia Eng.*, vol. 47, pp. 438–441, Sep. 2012. doi: 10.1016/j.proeng.2012.09.178.

[5] D. Obeid, S. Sadek, G. Zaharia, and G. El Zein, "Multitunable microwave system for touchless heartbeat detection and heart rate variability extraction," *Microw. Opt. Technol. Lett.*, vol. 52, pp. 192–198, Jan. 2010. doi: 10.1002/mop.24877.

[6] S. R. M. Shah, J. Velander, P. Mathur, M. D. Perez, N. B. Asan, D. G. Kurup, T. J. Blokhuis, and R. Augustine, "Split-ring resonator sensor penetration depth assessment using *in vivo* microwave reflectivity and ultrasound measurements for lower extremity trauma rehabilitation," *Sensors*, vol. 18, no. 2, p. 636, Feb. 2018. doi: 10.3390/s18020636.

[7] S. Raman, R. Augustine, and A. Rydberg, "Noninvasive osseointegration analysis of skull implants with proximity coupled split ring resonator antenna," *IEEE Trans. Antennas Propag.*, vol. 62, no. 11, pp. 5431–5436, Nov. 2014. doi: 10.1109/TAP.2014.2350522.

[8] S. R. M. Shah, J. Velander, P. Mathur, M. D. Perez, N. B. Asan, D. G. Kurup, T. Blokhuis, and R. Augustine, "Penetration depth evaluation of split ring resonator sensor using *in-vivo* microwave reflectivity and ultrasound measurements" in *Proc. 12th Eur. Conf. Antennas Propag. (EuCAP)*, London, U.K., Apr. 2018, pp. 1–4. doi: 10.1049/cp.2018.0500.

[9] M. D. Perez, S. R. M. Shah, J. Velander, M. Raaben, N. B. Asan, T. Blokhuis, and R. Augustine, "Microwave sensors for new approach in monitoring hip fracture healing," in *Proc. 11th Eur. Conf. Antennas Propag. (EuCAP)*, Paris, France, Mar. 2017, pp. 1838–1842. doi: 10.23919/EuCAP.2017.7928698.

[10] M. D. Perez, S. R. M. Shah, and R. Augustine, "Effective permittivity and frequency of resonance in single-split microstrip single-ring resonator for biomedical microwave sensor," in *Proc. IEEE Conf. Antenna Meas. Appl. (CAMA)*, Vasteras, Sweden, Sep. 2018, pp. 1–3. doi: 10.1109/CAMA.2018.8530591.

[11] S. R. M. Shah, J. Velander, M. D. Perez, L. Joseph, V. Mattsson, N. B. Asan, F. Huss, and R. Augustine, "Improved sensor for non-invasive assessment of burn injury depth using microwave reflectometry," in *Proc. 13th Eur. Conf. Antennas Propag. (EuCAP)*, Krakow, Poland, Mar./Apr. 2019, pp. 1–5.

[12] M. D. Perez, G. G. Thomas, S. R. M. Shah, J. Velander, N. B. Asan, P. Mathur, M. Nasir, D. Nowinski, D. Kurup, and R. Augustine, "Preliminary study on microwave sensor for bone healing follow-up after cranial surgery in newborns," in *Proc. 12th Eur. Conf. Antennas Propag. (EuCAP)*, London, U.K., Apr. 2018, pp. 1–4. doi: 10.1049/cp.2018.1250.

[13] M. D. Perez, V. Mattson, S. R. M. Shah, J. Velander, N. B. Asan, P. Mathur, M. Nasir, D. Nowinski, D. Kurup, and R. Augustine, "New approach for clinical data analysis of microwave sensor based bone healing monitoring system in craniosynostosis treated pediatric patients," in *Proc. IEEE Conf. Antenna Meas. Appl. (CAMA)*, Västerås, Sweden, Sep. 2018, pp. 1–3. doi: 10.1109/CAMA.2018.8530485.

[14] M. Raaben, S. R. M. Shah, R. Augustine, and T. J. Blokhuis, "Innovative measurement of rehabilitation progress in elderly with a hip fracture: A new endpoint," in *Proc. IEEE Conf. Antenna Meas. Appl. (CAMA)*, Västerås, Sweden, Sep. 2018, pp. 1–4. doi: 10.1109/CAMA.2018.8530474.

[15] M. D. Perez, S. R. M. Shah, and R. Augustine, "Effective permittivity and frequency of resonance in single-split microstrip single-ring resonator for biomedical microwave sensor," in *Proc. IEEE Conf. Antenna Meas. Appl. (CAMA)*, Västerås, Sweden, Sep. 2018, pp. 1–4. doi: 10.1109/CAMA.2018.8530591.

[16] B. J. Mohammed, A. M. Abbosh, S. Mustafa, and D. Ireland, "Microwave system for head imaging," *IEEE Trans. Instrum. Meas.*, vol. 63, no. 1, pp. 117–123, Jan. 2014.

[17] D. M. Pham and S. M. Aziz, "A real-time localization system for an endoscopic capsule using magnetic sensors," *Sensors*, vol. 14, no. 11, pp. 20910–20929, Nov. 2014. doi: 10.3390/s141120910.

[18] S. Y. Semenov, A. E. Bulyshev, A. Abubakar, V. G. Posukh, Y. E. Sizov, A. E. Souvorov, P. M. van den Berg, and T. C. Williams, "Microwave-tomographic imaging of the high dielectric-contrast objects using different image-reconstruction approaches," *IEEE Trans. Microw. Theory Techn.*, vol. 53, no. 7, pp. 2284–2294, Jul. 2005. doi: 10.1109/TMTT.2005.850459.

[19] Nello Carrara, Florance, Italy. *IFAC-CNR*. Accessed: May 13, 2019. [Online]. Available: http://niremf.ifac.cnr.it

[20] S. Gabriel, R. W. Lau, and C. Gabriel, "The dielectric properties of biological tissues: II. Measurements in the frequency range 10 Hz to 20 GHz," *Phys. Med. Biol.*, vol. 41, no. 11, pp. 2251–2269, Dec. 1996. doi: 10.1088/0031-9155/41/11/002.

[21] C. A. da G. Lopes, "Characterisation of the radio channel in on-body communications," Ph.D. dissertation, Higher Tech. Inst., Telecommun. Inst., Tech. Univ. Lisbon, Lisbon, Portugal, Nov. 2010.

[22] R. Augustine, "Electromagnetic modelling of human tissues and its application on the interaction between antenna and human body in the BAN context," Ph.D. dissertation, Laboratoire ESYCOM-Electronique, Systèmes de communication et Microsystèmes, Univ. Paris-Est, Paris, France, Jul. 2009.

[23] W. C. Chew, *Waves and Fields in Inhomogenous Media*, vol. 2, 1st ed. Hoboken, NJ, USA: Wiley, 1995, ch. 2, secs. 1–3, pp. 49–53.

[24] J. A. Kong, *Theory of Electromagnetic Waves*, 1st ed. New York, NY, USA: Wiley, 1975, p. 339.

[25] E. Anemogiannis and E. N. Glytsis, "Multilayer waveguides: Efficient numerical analysis of general structures," *J. Lightw. Technol.*, vol. 10, no. 10, pp. 1344–1351, Oct. 1992.

SYAIFUL REDZWAN MOHD SHAH was born in Malaysia, in 1984. He received the B.Eng. degree in electronic engineering (telecommunication electronics) and the M.Sc. degree in communication and computer from the Universiti Teknikal Malaysia Melaka, Durian Tunggal, Malaysia, in 2007 and 2010, respectively. He is currently pursuing the Ph.D. degree with the Ångström Laboratories, Solid State Electronics Division, Microwaves in Medical Engineering Group, Department of Engineering Sciences, Uppsala University (UU), Sweden. From 2011 to 2013, he was a Research Engineer with Huawei Technologies, Malaysia. He was with the LG CNS Ltd., Malaysia, as a Senior Research Engineer, from 2013 to 2015. His current research interests include designing BMD sensors, microwave material characterization, noninvasive diagnostics, and biomedical sensors.

NOOR BADARIAH ASAN (S'17) was born in Malaysia, in 1984. She received the B.Eng. degree in electronic engineering (telecommunication electronics) from the Universiti Teknikal Malaysia Melaka, Malaysia, in 2008, and the M.Eng. degree in communication and computer from the National University of Malaysia, Selangor, Malaysia, in 2012. She is currently pursuing the Ph.D. degree with the Ångström Laboratories, Department of Engineering Sciences, Uppsala University. In 2010, she joined the Department of Electronic and Computer Engineering, Universiti Teknikal Malaysia Melaka, as a Lecturer. She is involved in characterizing and developing the fat-intrabody microwave communication (Fat-IBC). Her current research interests include wireless sensor networks, material characterization, and designing, optimizing, and characterizing biomedical sensor for intrabody area networks.

JACOB VELANDER was born in Uppsala, Sweden, in 1981. He received the B.Sc. degree in electrical engineering and the M.Sc. degree in technology from the Department of Engineering Sciences, Uppsala University (UU), Sweden, in 2015 and 2016, respectively. He was a Project Assistant of low frequency simulations with the Department of Engineering Sciences, Solid State Electronics, UU. He is currently pursuing the Ph.D. degree with Ångström Laboratories, Solid State Electronics Division, Microwaves Medical Engineering Group, Department of Engineering Sciences, UU. In parallel, he is involved in two projects, namely, bone density analysis system (BDAS) and Senseburn. He mainly focused on monitoring bone mineral density and degree of skin burn. His current research interests include artificial models (phantoms) fabrication for Craniosynostosis and skin burn. He is also involved in BMD sensor development, CST simulations, and body tissue characterizations in ex-vivo and in-vivo context.

JAVAD EBRAHIMIZADEH was born in Iran, in 1989. He received the B.S. degree in electrical engineering from the University of Sistan and Baluchestan, Zahedan, Iran, in 2011, and the M.S. degree in electrical engineering from Tehran University, Tehran, Iran, in 2015. His current research interests include applied electromagnetics, radio remote sensing, electromagnetic wave propagation, scattering, and microwave imaging systems.

MAURICIO D. PEREZ was born in Buenos Aires, Argentina, in 1980. He received the Engineering degree in electronics from the National Technological University (UTN), Argentina, in 2007, and the Ph.D. degree in electrical engineering from the University of Bologna (UNIBO), Italy, in 2012. He was an Industrial Researcher in Italy, from 2012 to 2014, and an Academic Teacher and Researcher with UTN, from 2014 to 2017. He is currently a Teacher and a Researcher with the Ångström Laboratories, Microwaves in Medical Engineering Group (MMG), Uppsala University (UU), Sweden. His current research interest includes modeling and data-driven validation of microwave sensors for biomedical applications.

VIKTOR MATTSSON was born in Åland Islands, Finland, in 1992. He received the M.Sc. degree in scientific computing from the Engineering Physics Program, Uppsala University, Sweden, in 2018, where he is currently pursuing the Ph.D. degree with Ångström Laboratories, Solid State Electronics Division, Microwaves in Medical Engineering Group, Department of Engineering Sciences. His current research interests include data analysis, modeling microwave sensors, and biomedical applications.

TACO BLOKHUIS received the degree in medicine in Amsterdam, The Netherlands, in 1996, and the Ph.D. degree, in 2001. After finishing his training as a Trauma Surgeon, he has been working with university medical centers throughout The Netherlands. In 2014, he was appointed as an Associate Professor with the University of Utrecht, The Netherlands. He is currently with the Maastricht University Medical Center, The Netherlands. His current research interest includes basic (preclinical) research.

ROBIN AUGUSTINE received the bachelor's degree in electronics science from Mahatma Gandhi University, Kottayam, India, in 2003, the master's degree in electronics from the Cochin University of Science and Technology, Cochin, India, in 2005, and the Ph.D. degree in electronics and optronics systems from the Université de Paris Est Marne La Vallée, France, in 2009. He did the postdoctoral training with the University of Rennes 1, IETR, from 2009 to 2011. Since 2011, he has been a Senior Researcher with Uppsala University, Sweden. In 2016, he was appointed as a Docent (Associate Professor) in microwave technology with Uppsala University. He is the Swedish PI of the Eureka Eurostars project COMFORT and Indo-Swedish Vinnova-DST funded project BDAS. He received the Grant from the Swedish Research Council (VR) for his project Osteodiagnosis. He is also a WP Leader of the H2020 project SINTEC and Co-PI of the framework project LifeSec from the Swedish Strategic Foundation (SSF). He is responsible for the lead technical development in the Eurostars project SenseBurn. He is currently leading the Solid State Electronics Division, Microwaves in Medical Engineering Group (MMG), Uppsala University. He is the author or coauthor of more than 110 publications, including journals and conferences in the field of sensors, microwave antennas, bioelectromagnetics, and material characterization.

• • •